ISSN 1027-4510, Journal of Surface Investigation: X-ray, Synchrotron and Neutron Techniques, 2024, Vol. 18, No. 2, pp. 274–280. © Pleiades Publishing, Ltd., 2024.

Simulating Quantum States of Positively Charged Particles Channeling along the [111] Direction in a Silicon Crystal

V. V. Syshchenko[a], *, A. I. Tarnovsky[b], A. S. Parakhin[a], and A. Yu. Isupov[b]

[a] *Belgorod State University, Belgorod, 308015 Russia*

[b] *Joint Institute for Nuclear Research, Dubna, Moscow oblast, 141980 Russia*

**e-mail: syshch@yandex.ru*

Received July 26, 2023; revised September 29, 2023; accepted September 29, 2023

Abstract—The potential well formed by the repulsive continuous potentials of three neighboring [111] chains in a silicon crystal, for a positively charged particle, exhibits the symmetry of an equilateral triangle, described by the C_{3v} group. In this case, the previously developed procedure for finding the eigenvalues of the transverse motion energy of channeled positively charged particles (positrons or protons) and the corresponding eigenfunctions of the Hamiltonian, implemented on a square spatial grid, leads to artifacts in numerical modeling. We present a modification of the modeling algorithm based on a hexagonal grid, which takes into account the symmetry of the problem. The results of both approaches are compared, demonstrating the absence of artifacts when using a hexagonal grid. Using numerical methods, all discrete energy levels of the transverse motion of channeled positrons with a longitudinal motion energy of 2, 2.5, 3, 3.5, and 4 GeV in the discussed potential well are found. The developed procedure can be used in studies of manifestations of dynamic tunneling and quantum chaos in channeling.

Keywords: channeling, silicon, numerical simulation, spectral method, hexagonal grid, quantum chaos

DOI: 10.1134/S1027451024020186

INTRODUCTION

A fast charged particle moving near one of the densely packed crystallographic axes in a crystal can be trapped in the potential well formed by these axes, undergoing finite motion in the plane perpendicular to the corresponding axis and anomalously penetrating deep into the crystal. This phenomenon is known as axial channeling [1–4]. Particle motion in the axial-channeling mode can be accurately described as motion in the field of a continuous potential of the atomic chain, i.e., a potential averaged along the chain axis [5]. For such a potential, the longitudinal component of the particle momentum $p_{\|}$ is conserved, which reduces the problem of particle motion to a two-dimensional problem of motion in the transverse plane.

When fast particles channel in crystals, quantum effects can manifest itself [1]. In a series of previous works [6–14], a numerical method was developed to find the energy levels of two-dimensional transverse motion and the corresponding wave functions of steady states of electrons and positrons channeled in the [110] and [100] directions of a silicon crystal. In this work, a quantum description of the transverse motion of positrons in the [111] direction of a silicon crystal is provided, which required some modification of the numerical method for the potential well formed by the continuous potentials of three neighboring chains in the [111] direction of the crystal. Nonphysical artifacts arising from numerical integration of the Schrödinger equation with such a potential on a square discrete grid are discussed. It is shown that the use of a hexagonal grid, taking into account the symmetry of the potential, leads to the elimination of these drawbacks.

EXPERIMENTAL

The motion of a relativistic particle in a crystal at a small angle to a densely packed crystallographic axis can be described as two-dimensional motion in the transverse plane (with respect to this axis) under the action of continuous potentials averaged along atomic chains perpendicular to this plane while preserving the longitudinal component of particle momentum $p_{\|}$. In the (111) plane of a silicon crystal, such chains form a hexagonal lattice with a side of the primitive cell $a = a_z/\sqrt{6} \approx 2.217$ Å, where a_z is the period of the silicon lattice. For a positively charged particle (hereafter, for specificity, we refer to a positron), the continuous potential of the chain is repulsive. However, near the center of the triangle, at the vertices of which the three closest chains are located, a small potential well arises (Fig. 1). In this well, there is the possibility of finite motion of the positron in the transverse plane, known as axial channeling. The potential energy of the posi-

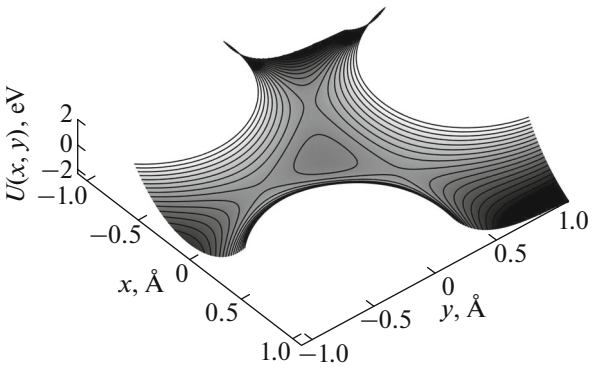

Fig. 1. Potential energy (1) of a positron moving along the [111] direction of a silicon crystal.

tron, taking into account the contributions from these three chains, can be described by the following sum:

$$U(x,y) = U_1\left(x, y - \frac{a}{\sqrt{3}}\right) + U_1\left(x + \frac{a}{2}, y + \frac{a}{2\sqrt{3}}\right) + U_1\left(x - \frac{a}{2}, y + \frac{a}{2\sqrt{3}}\right) - 7.8571\ \text{eV}, \quad (1)$$

where the constant is selected to make the potential zero at the center of the triangle. The continuous potential of an individual atomic chain is approximated by the equation [1]

$$U_1(x,y) = U_0 \ln\left(1 + \frac{\beta R^2}{x^2 + y^2 + \alpha R^2}\right), \quad (2)$$

where, for the [111] chain of silicon, $U_0 = 58.8$ eV, $\alpha = 0.37$, $\beta = 2.0$, and $R = 0.194$ Å (Thomas–Fermi radius). The quantum dynamics of the transverse motion of a positron in the axial channeling mode is described by the two-dimensional Schrödinger equation

$$\hat{H}\Psi(x,y,t) = i\hbar\frac{\partial}{\partial t}\Psi(x,y,t) \quad (3)$$

with the Hamiltonian

$$\hat{H} = -\frac{c^2\hbar^2}{2E_\parallel}\left(\frac{\partial^2}{\partial x^2} + \frac{\partial^2}{\partial y^2}\right) + U(x,y) \equiv \hat{T}_{\text{kin}} + \hat{U}, \quad (4)$$

where the quantity $E_\parallel/c^2$ plays the role of the particle mass, and $E_\parallel = (m^2c^4 + p_\parallel^2c^2)^{1/2}$ represents the energy of longitudinal motion [1].

The integration of Eq. (3) with potential (1) is possible numerically only. The basis of our approach is the so-called spectral method for finding eigenvalues and eigenvectors of the Hamiltonian [15], the details of which, applied to the channeling problem, are described in [6–10]. This method relies on computing the correlation function between wave functions of the system at the initial and current moments in time

$$P(t) = \int_{-\infty}^{\infty}\int_{-\infty}^{\infty}\Psi^*(x,y,0)\Psi(x,y,t)\,dxdy, \quad (5)$$

the Fourier transform of which contains information about the eigenvalues of the Hamiltonian. Thus, the procedure is based on numerical simulation of the time evolution of the wave function according to Eq. (3):

$$\Psi(x,y,t+dt) = \exp\left(-i\frac{dt}{\hbar}\hat{H}\right)\Psi(x,y,t). \quad (6)$$

Derivation based on Eq. (6) is complicated by the fact that the Hamiltonian (4) consists of two noncommuting terms. The first term (corresponding to the kinetic energy) is diagonal in the momentum representation, while the second term (corresponding to the potential energy) is diagonal in the coordinate representation. In this case, the operator-splitting method is used, based on the Zassenhaus product formula [15–17]:

$$\exp\left(-i\frac{\Delta t}{\hbar}\left(\hat{T}_{\text{kin}} + \hat{U}\right)\right) = \exp\left(-i\frac{\Delta t}{2\hbar}\hat{U}\right) \times \exp\left(-i\frac{\Delta t}{\hbar}\hat{T}_{\text{kin}}\right)\exp\left(-i\frac{\Delta t}{2\hbar}\hat{U}\right)\left(1 + \mathbb{O}\left((\Delta t)^3\right)\right).$$

To apply the "kinetic" evolution operator, the function on which it acts must be represented as an expansion in the eigenfunctions of such an operator, i.e., in a Fourier series. In the numerical procedure developed earlier [6–14], the wave function was defined in a square spatial domain on a square discrete grid, and the Fourier expansion was performed trivially. However, such an approach does not correspond to the symmetry of the problem considered here and leads to artifacts in numerical simulation. The problem can be addressed by selecting a hexagonal grid and defining the wave function and potential in the region as a regular hexagon (Fig. 2), the center of which coincides with the center of the triangular well formed by potential (1).

To represent the function as a Fourier series in this case, we use the well-known concept of the reciprocal lattice in solid-state physics (for example, [18, 19]):

$$\Psi(\mathbf{r}) = \sum_m \Psi_m \exp(i\mathbf{G}_m\cdot\mathbf{r}) = \sum_{m_1=-\infty}^{\infty}\sum_{m_2=-\infty}^{\infty}\Psi_{m_1,m_2}\exp\left(i(m_1\mathbf{g}_1 + m_2\mathbf{g}_2)\cdot\mathbf{r}\right), \quad (7)$$

where the basis vectors of the reciprocal lattice $\mathbf{g}_1$ and $\mathbf{g}_2$ are constructed based on the direct lattice $\mathbf{a}_1$, $\mathbf{a}_2$, and $\mathbf{a}_3$, and in the case of a two-dimensional lattice, vector $\mathbf{a}_3$ is selected as the unit vector perpendicular to the plane containing $\mathbf{a}_1$ and $\mathbf{a}_2$:

$$\mathbf{g}_1 = 2\pi\frac{\mathbf{a}_2\times\mathbf{a}_3}{\mathbf{a}_1\cdot(\mathbf{a}_2\times\mathbf{a}_3)}, \quad \mathbf{g}_2 = 2\pi\frac{\mathbf{a}_3\times\mathbf{a}_1}{\mathbf{a}_1\cdot(\mathbf{a}_2\times\mathbf{a}_3)}. \quad (8)$$

Representing a function as a Fourier series can be performed either for a periodic function or for a function defined in a bounded region of space. In the case under consideration, this region, in the form of a regular hexagon, plays the role of the Wigner–Seitz cell in real space, and the vectors $\mathbf{a}_1$ and $\mathbf{a}_2$ serve as its translation vectors.

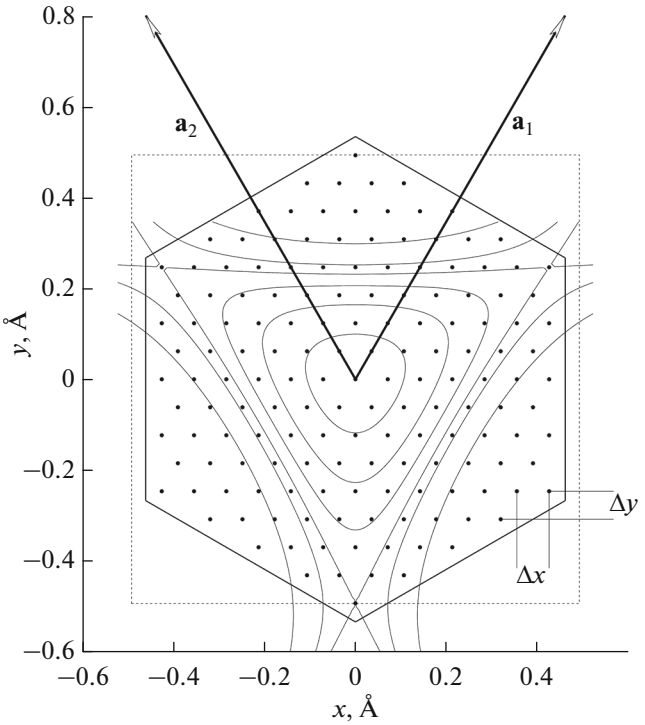

Fig. 2. Schematic representation of a hexagonal grid for numerical simulation in configuration space (the value $N = 13$ was selected to plot the figure).

Assigning a function on a discrete grid within such a cell, according the Nyquist–Kotelnikov–Shannon theorem, leads to a limitation of the function's spectrum in reciprocal space, i.e., to a limitation of the summation in Eq. (7) within the limits of

$$-(N-1) \le m_{1,2} \le N-1, \tag{9}$$

where $N = |\mathbf{a}_{1,2}|/\Delta x$ is the number of rows in the hexagonal grid in coordinate space, which aligns along the vector $\mathbf{a}_1$ or $\mathbf{a}_2$. It is convenient to choose this number as odd, and the grid itself in such a way that its central node coincides with the center of the triangular potential well (1). The reciprocal lattice vectors in Eq. (7) define a hexagonal grid in reciprocal space, and condition (9) limits the Bravais lattice in the form of a rhombus (circles in Fig. 3). Parallel translations of individual nodes of this grid by vectors $\pm N\mathbf{g}_{1,2}$ do not violate the validity of expansion (7) and enable constructing, instead of the Bravais lattice, the Wigner–Seitz cell in the form of a regular hexagon (dots in Fig. 3), which best corresponds to the conditions of the problem. In the calculations, we used a hexagonal grid in coordinate space with $N = 115$ and a step of $\Delta x \approx 0.0075$ Å. For comparison, simulation was also performed for a square grid with $N = 128$ and a step of $\Delta x \approx 0.0077$ Å, and the corresponding spatial region is marked with a dashed line in Fig. 2.

Fourier transformation of the correlation function (5) reveals the energy only of those steady states that leave

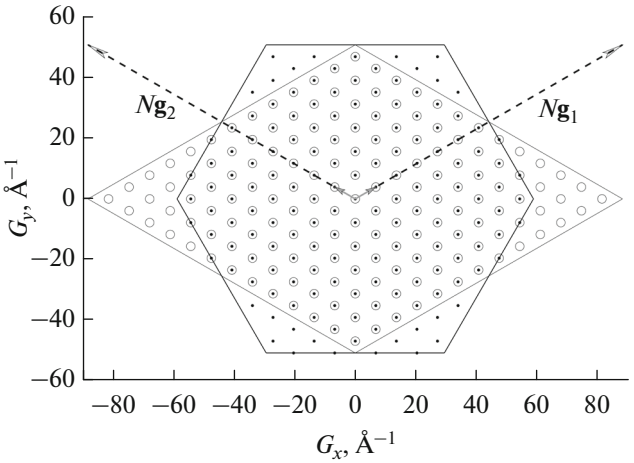

Fig. 3. Schematic representation of a hexagonal grid for numerical simulation in reciprocal space for $N = 13$.

the initial wave packet $\Psi(x, y, 0)$ in superposition. If we select an asymmetric Gaussian

$$\Psi(x,y,0) = \psi_0(x,y) = \frac{1}{\pi\sigma_x\sigma_y}\exp\left(-\frac{(x-x_0)^2}{2\sigma_x^2} - \frac{(y-y_0)^2}{2\sigma_y^2}\right), \tag{10}$$

it contains all steady states in the well. However, to investigate the spectrum of the Hamiltonian (4), its eigenstates need to be classified according to the symmetry properties of potential (1).

Since potential (1) has the symmetry of an equilateral triangle, all available states of transverse motion can be classified into irreducible representations of the group C_{3v} (or an isomorphic group D_3 (for example, [20])), depending on the symmetry type of the wave function. The group elements include the identity transformation I, rotations at angles $2\pi/3$ and $4\pi/3$, denoted by R and R^2, reflection in the "vertical" plane P, and the combinations PR and PR^2. This group has two one-dimensional irreducible representations, denoted as A_1 and A_2, which correspond to nondegenerate energy levels, and one two-dimensional representation, denoted as E, corresponding to doubly degenerate levels. The basis function of the irreducible representation A_1 remains unchanged for all transformations. It is easy to construct the initial wave packet satisfying this requirement based on the results of the action on (10) of all group operators, summed with equal weights:

$$\psi^{(A_1)} = \psi_0 + R\psi_0 + R^2\psi_0 + P\psi_0 + PR\psi_0 + PR^2\psi_0. \tag{11}$$

A function changing sign upon reflection,

$$\psi^{(A_2)} = \psi_0 + R\psi_0 + R^2\psi_0 - P\psi_0 - PR\psi_0 - PR^2\psi_0, \tag{12}$$

forms the basis of the representation A_2. The basis of the two-dimensional irreducible representation E consists of linear combinations with complex coefficients,

$$\psi_1^{(E)} = \psi_0 + \exp\left(\frac{2\pi i}{3}\right) R\psi_0 + \exp\left(4\pi i/3\right) R^2\psi_0 + P\psi_0 + \exp\left(-2\pi i/3\right) PR\psi_0 + \exp\left(-4\pi i/3\right) PR^2\psi_0, \quad (13)$$

$$\psi_2^{(E)} = \psi_1^{(E)*}. \quad (14)$$

These functions transform into each other upon reflections and acquire a phase factor upon rotations. However, with further consideration of the intended use of the developing procedure in the search for quasi-classically interpretable wave functions (similar to what was done in [14] for positron channeling in the

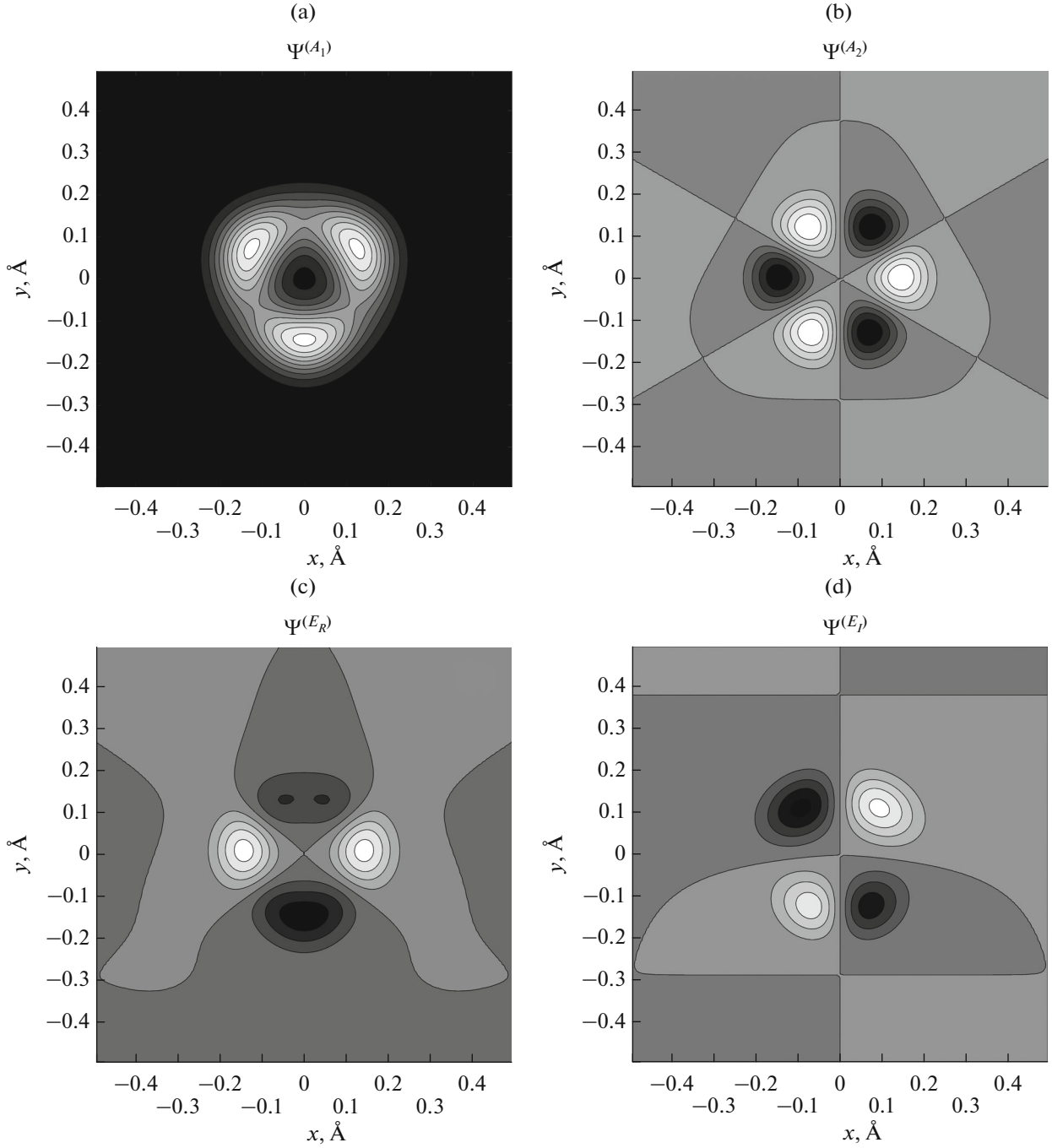

Fig. 4. Graphs of the initial functions included in the numerical simulation, related to symmetry (a) A_1, Eq. (11); (b) A_2, Eq. (12); (c) E_R, Eq. (15); (d) E_I, Eq. (15).

Table 1. Energy levels of transverse motion (eV) in the potential well (1), found numerically with discrete specification of functions on square and hexagonal grids

Square grid			Hexagonal grid		
A_1	E_R	E_I	A_1	E_R	E_I
$E_\parallel = 2$ GeV					
0.13020			0.13022		
(0.25466)	0.25467	0.25467		0.25507	0.25507
$E_\parallel = 2.5$ GeV					
0.11648			0.11649		
(0.22822)	0.22846	0.22845		0.22858	0.22858
0.32355	(0.32355)		0.32594		
$E_\parallel = 3$ GeV					
0.10635			0.10636		
(0.20865)	0.20900	0.20899		0.20904	0.20904
0.29783	(0.29792)		0.29879		
(0.31292)	0.31297	0.31295		0.31360	0.31360
$E_\parallel = 3.5$ GeV					
0.09848			0.09848		
	0.19381	0.19380		0.19382	0.19382
0.27743	(0.27768)		0.27783		
(0.29021)	0.29045	0.29043		0.29071	0.29071
$E_\parallel = 4$ GeV					
0.09213			0.09213		
	0.18152	0.18152		0.18153	0.18153
0.26075			0.26093		
(0.27199)	0.27218	0.27217		0.27229	0.27229

Nonphysical artifacts are indicated in parentheses. Underlined values are the nonphysical splitting of degenerate levels.

[100] direction), it is convenient to take the real and imaginary parts (13) as the initial functions,

$$\psi^{(E_R)} = \mathrm{Re}\,\psi_1^{(E)}, \quad \psi^{(E_I)} = \mathrm{Im}\psi_1^{(E)}, \qquad (15)$$

since a complete set of eigenfunctions of a real Hamiltonian can always be selected to be real (for example, [21]). Substituting the initial functions in the form of (11), (12), or one of (15) into (5) and performing the numerical procedure result in finding the eigenvalues of the energy of bound states in the potential well (1), corresponding to the eigenfunctions of the Hamiltonian with symmetry of the respective type. Plots of the initial functions with the symmetry of all four types (11), (12), and (15) are presented in Fig. 4.

RESULTS AND DISCUSSION

As mentioned earlier, parameter $E_\parallel/c^2$ in Hamiltonian (4) plays the role of the particle mass, so with an increase in the energy of longitudinal motion, the total number of energy levels in the potential well increases. This can be easily understood by considering quasiclassical arguments (for example, [1]); new levels "squeeze" into the potential well from the continuum of states lying above it, representing infinite particle motion. Table 1 presents the results of the numerical determination of transverse-motion energy levels for various values of $E_\parallel$. It turns out that these values of longitudinal-motion energy are not enough to have at least one bound state in the well with symmetry of type A_2.

The data in Table 1 suggest that simulation using a square grid, in addition to revealing true eigenvalues of positron energy in the well (1), generates artifacts of two kinds. First, the algorithm that uses initial functions related to one of the two types of symmetry: A_1 or E_R ((11) and (15)), returns some false levels in the results of the simulation, coinciding with the true levels related to the second type (which can be verified by constructing the corresponding eigenfunction of the Hamiltonian for that energy value). All such false eigenvalues are marked in the table in parentheses.

Their appearance is because the function specified for a square grid does not have undisturbed symmetry of A_1 or E_R and represents a superposition of functions of both types.

Another type of artifact is the observed nonphysical splitting near the upper edge of the well of the doubly degenerate E-type level. It is related to the fact that the specified potential in the square region does not actually have C_{3v} symmetry, and this symmetry is violated beyond the triangular well for the highest-lying states. In Table 1, all such split eigenvalues are underlined. This is also the reason for the increase from the bottom to the top of the well in the difference in the absolute values of the energy levels found on square and hexagonal grids.

Simulation using a hexagonal grid avoids both of the described drawbacks.

CONCLUSIONS

The paper examines the channeling of positrons with energies ranging from 2 to 4 GeV along the [111] direction of a silicon crystal. The quantum energy levels of the transverse motion of positrons in this case can only be numerically determined, implying the specification of the particle potential energy and its wave function on a discrete spatial grid. The specificity of the problem under consideration lies in the fact that three neighboring atomic chains [111] create a potential well with the symmetry of an equilateral triangle. Under these conditions, the use of a square grid leads to the appearance of nonphysical artifacts alongside the true energy levels in the simulation results. The developed modification of the spectral method for finding eigenvalues of transverse-motion energy, using a hexagonal grid, eliminates these drawbacks.

Interest in the quantum description of motion in a potential well with the symmetry of an equilateral triangle is associated with the fact that the phenomenon of dynamic tunneling was investigated precisely in such a well in the pioneering work [22]. Dynamic tunneling during channeling in a well of another configuration (with the symmetry C_{4v} of a square) was studied in [14].

It is also worth noting that the quantum description of particle motion in planar and axial channels represents an interesting problem, illustrating the manifestation of quantum mechanics beyond standard academic pursuits and possessing significant pedagogical potential, as emphasized in [23, 24].

FUNDING

This work was supported by ongoing institutional funding. No additional grants to carry out or direct this particular research were obtained.

CONFLICT OF INTEREST

The authors of this work declare that they have no conflicts of interest.

REFERENCES

1. A. I. Akhiezer and N. F. Shulga, *Electrodynamics of High Energies in Matter* (Nauka, Moscow, 1993) [in Russian].
2. A. I. Akhiezer, N. F. Shul'ga, V. I. Truten', A. A. Grinenko, and V. V. Syshchenko, Phys.-Usp. **38**, 1119 (1995). https://doi.org/10.1070/PU1995v038n10ABEH000114
3. D. S. Gemmel, Rev. Mod. Phys. **46**, 129 (1974). https://doi.org/10.1103/RevModPhys.46.129
4. U. I. Uggerhøj, Rev. Mod. Phys. **77**, 1131 (2005). https://doi.org/10.1103/RevModPhys.77.1131
5. J. Lindhard, K. Dan. Vidensk. Selsk., Mat.-Fys. Skr. **34** (14), 1 (1965).
6. Shul'ga, N.F., V. V. Syshchenko, and V. S. Neryabova, J. Surf. Invest.: X-ray, Synchrotron Neutron Tech. **7**, 279 (2013). https://doi.org/10.1134/S1027451013020183
7. N. F. Shul'ga, V. V. Syshchenko, and V. S. Neryabova, Nucl. Instrum. Methods Phys. Res., Sect. B **309**, 153 (2013). https://doi.org/10.1016/j.nimb.2013.01.022
8. N. F. Shul'ga, V. V. Syshchenko, A. I. Tarnovsky, A. Yu. Isupov, J. Surf. Invest.: X-ray, Synchrotron Neutron Tech. **9**, 721 (2015). https://doi.org/10.1134/S1027451015040199
9. N. F. Shul'ga, V. V. Syshchenko, A. I. Tarnovsky, and A. Yu. Isupov, Nucl. Instrum. Methods Phys. Res., Sect. B **370**, 1 (2016). https://doi.org/10.1016/j.nimb.2015.12.040
10. N. F. Shul'ga, V. V. Syshchenko, A. I. Tarnovsky, and A. Yu. Isupov, J. Phys.: Conf. Ser. **732**, 012028 (2016). https://doi.org/10.1088/1742-6596/732/1/012028
11. V. V. Syshchenko and A. I. Tarnovsky, J. Surf. Invest.: X-ray, Synchrotron Neutron Tech. **15**, 728 (2021). https://doi.org/10.1134/S1027451021040200
12. V. V. Syshchenko, A. I. Tarnovsky, A. Yu. Isupov, and I. I. Solovyev, J. Surf. Invest.: X-ray, Synchrotron Neutron Tech. **14**, 306 (2020). https://doi.org/10.1134/S1027451020020354
13. N. F. Shul'ga, V. V. Syshchenko, A. I. Tarnovsky, V. I. Dronik, and A. Yu. Isupov, J. Instrum. **14**, C12022 (2019). https://doi.org/10.1088/1748-0221/14/12/C12022
14. V. V. Syshchenko, A. I. Tarnovsky, V. I. Dronik, A. Yu. Isupov, J. Surf. Invest.: X-ray, Synchrotron Neutron Tech. **15**, 73 (2022). https://doi.org/10.1134/S1027451022020203
15. M. D. Feit, J. A. Fleck, and A. Steiger, J. Comput. Phys. **47**, 412 (1982). https://doi.org/10.1016/0021-9991(82)90091-2

16. D. Scholz and M. Weyrauch, J. Math. Phys. **47**, 033505 (2006). https://doi.org/10.1063/1.2178586

17. V. V. Serov, *Numerical Methods for Solving Non-Stationary Quantum Mechanical Problems* (Novyi Veter, Saratov, 2011) [in Russian].

18. Ch. Kittel, *Introduction to Solid State Physics* (John Wiley and Sons, 2005; Nauka, Moscow, 1978).

19. V. V. Syshchenko and V. G. Syshchenko, *Solid State Theory for Beginners* (Regul. Khaoticheskaya Din., Inst. Komp. Issled., Moscow, Izhevsk, 2022) [in Russian].

20. L. D. Landau and E. M. Lifshits, *Theoretical Physics* (Fizmatlit, Moscow, 2016), **Vol. 3** [in Russian].

21. H.-J. Stockmann, Quantum Chaos (Cambridge Univ. Press, Cambridge, 2000; Fizmatlit, Moscow, 2004).

22. M. J. Davis and E. J. Heller, J. Chem. Phys. **75**, 246 (1981). https://doi.org/10.1063/1.441832

23. N. P. Kalashnikov, A. S. Olchak, J. Surf. Invest.: X-ray, Synchrotron Neutron Tech. **16**, 659 (2022). https://doi.org/10.1134/S1027451022030132

24. N. P. Kalashnikov, A. S. Olchak, J. Surf. Invest.: X-ray, Synchrotron Neutron Tech. **16**, 914 (2022). https://doi.org/10.1134/S1027451022040279

Translated by O. Zhukova